

Spin Teleportation via Bell-Triplet States Emergent from Proton-Proton Scattering

Z. X. Shen,^{1,2} H. Y. Shang,^{1,2} Y. G. Ma^{1,2,3,*} D. Bai^{4,†}
 S. M. Wang^{1,2,‡} Z. C. Xu,^{1,2} Y. Ayyad^{5,§} and C. Filgueira⁵

¹Key Laboratory of Nuclear Physics and Ion-beam Application (MOE),
 Institute of Modern Physics, Fudan University, Shanghai 200433, China

²Shanghai Research Center for Theoretical Nuclear Physics,
 NSFC and Fudan University, Shanghai 200438, China

³School of Physics, East China Normal University, Shanghai 200241, China

⁴College of Mechanics and Engineering Science, Hohai University, Nanjing, 211100, China

⁵IGFAE, Universidade de Santiago de Compostela, E-15782, Santiago de Compostela, Spain

Entanglement is a key resource in quantum information science, yet its properties and applications in nuclear systems remain largely unexplored. Here, using proton-proton scattering as a quantum laboratory, we report the emergence of a near-pure Bell-triplet state at a laboratory energy of 151 MeV and a center-of-mass scattering angle of 90 degrees. In this unique kinematic regime, the scattering amplitude functions as a transition operator connecting distinct Bell states. Building upon this emergent resource, we propose a quantum teleportation protocol for proton spins, exploiting the intrinsic Hamiltonian of the strong interaction to perform the requisite Bell measurement. These findings effectively bridge few-body nuclear physics and quantum technology, establishing proton-proton scattering as both a source of high-fidelity entanglement and a natural processor for quantum information.

Introduction—Quantum entanglement is a curious yet fundamental resource of nature, characterized by strong nonlocal correlations with no classical description [1]. Harnessing this property is crucial for next-generation technologies ranging from quantum computing to quantum sensing [2]. While entanglement is routinely engineered in controlled systems like trapped ions [3–5], ultracold atoms [6–8], and superconducting circuits [9–11], it is also an inherent and ubiquitous feature across vastly different scales, from the subatomic world to theories of quantum gravity [12–17]. In this broader context, nuclear and particle systems—with rich spin-dependent dynamics—offer a natural arena for producing and manipulating spin-entangled states, and recent theory and measurements have begun to explore entanglement and Bell nonlocality in hadronic and electroweak reactions [14, 18–21]. Adopting this quantum-information perspective not only yields novel insights into nuclear forces, structure, and dynamics [18–36], but also drives innovations in experimental techniques for probing quantum correlations in nuclei [37].

As one of the most fundamental processes in nuclear physics, nuclear scattering serves as a primary tool for probing nuclear forces and structure [38, 39]. Interest in spin entanglement in this setting dates back to the pioneering nuclear Bell test [40], which exploited the spin-singlet state generated by low-energy proton-proton (pp) scattering. Owing to technical challenges, the field then entered a long hiatus, and a second Bell test using proton singlet pairs was not realized until 2006 [41]. More recently, this direction has seen substantial theoretical

progress, with several studies investigating the spin entanglement properties of np , nn , and neutron-deuteron scattering using the full S -matrix formalism [42–46]. In contrast, a parallel comprehensive investigation for the pp scattering—the experimentally most accessible two-nucleon channel—has remained incomplete, leaving a conspicuous gap in our understanding of spin entanglement across all nucleon-nucleon sectors.

In this work, we complement these efforts by focusing on pp scattering and show that it reveals physics not exposed by conventional observables alone. Although modern interactions reproduce pp differential cross sections up to ~ 350 MeV with $\chi^2/\text{dof} \sim 1$ [47–51], this apparent completeness does not extend to entanglement-sensitive structure. By adopting entanglement measures as quantum-information-inspired probes, we identify a unique, previously unreported kinematic region characterized by the emergence of a nearly pure Bell-triplet state. This window provides a new benchmark for constraining nucleon–nucleon interactions and a realistic venue for Bell-type tests. Moreover, by tracing the dynamical origin of this phenomenon, we find that the scattering amplitude effectively acts as a transition operator between Bell states, positioning nuclear scattering as a promising resource for quantum information processing.

As a concrete application enabled by this discovery, we propose a quantum teleportation protocol [52] for proton spins, driven directly by the intrinsic Hamiltonian of the strong interaction. In the identified kinematic window, the scattering amplitude effectively performs the requisite Bell measurement, enabling intact transfer of an unknown spin state between protons without externally engineered two-qubit gates. In this sense, teleportation is not merely a conceptual analogy but a novel experimental measurement modality—one that leverages entanglement generated by realistic nuclear forces to realize quantum-information tasks in the femtometer/MeV domain.

* Email: mayugang@fudan.edu.cn

† Email: dbai@hhu.edu.cn

‡ Email: wangsimin@fudan.edu.cn

§ Email: yassid.ayyad@usc.es

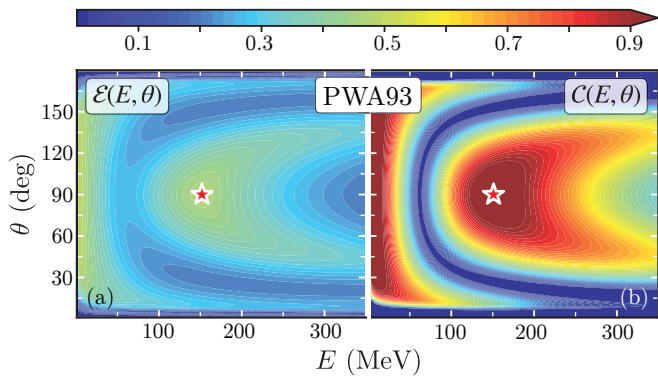


FIG. 1. (a) Entanglement power \mathcal{E} and (b) concurrence \mathcal{C} for pp scattering, shown as functions of the laboratory kinetic energy E and the center-of-mass angle θ . Both quantities are calculated from the Nijmegen PWA93 database, with the concurrence evaluated for a completely unpolarized initial state. The red pentagrams mark the second local maxima in each distribution at $(E, \theta) = (151 \text{ MeV}, 90^\circ)$.

Spin amplitude and entanglement measures—The two-proton system is described within the combined momentum-spin Hilbert space, $\mathcal{H} = \mathcal{H}_p \otimes \mathcal{H}_s$, where $\mathcal{H}_s = \mathcal{H}_A \otimes \mathcal{H}_B$ denotes the four-dimensional spin space for two spin- $\frac{1}{2}$ particles. With an initial spin density matrix ρ_i , the final state is $\rho_f = M\rho_i M^\dagger / \text{Tr}(M\rho_i M^\dagger)$. The spin amplitude M , which is a 4×4 matrix encoding the complete spin dependence of pp scattering, can be evaluated via the Nijmegen PWA93 database [47, 53] and chiral effective field theory (χ EFT) [54]. The Coulomb correction is incorporated following the treatment in Refs. [47, 55]. In all calculations, the z -axis is aligned with the initial relative momentum.

To quantify the spin entanglement properties of pp scattering, we employ entanglement power and concurrence. For a scattering event at laboratory kinetic energy E and center-of-mass angle θ , the entanglement power $\mathcal{E}(E, \theta)$ quantifies the average entanglement generated by the scattering operator acting on all possible separable initial spin states. These initial states are parameterized as

$$|\chi_i\rangle = \left[\cos \frac{\theta_1}{2}, e^{i\varphi_1} \sin \frac{\theta_1}{2} \right]^\top \otimes \left[\cos \frac{\theta_2}{2}, e^{i\varphi_2} \sin \frac{\theta_2}{2} \right]^\top,$$

where the angles define the initial spin orientations on the Bloch spheres of the two protons [56, 57]. The corresponding final state is $|\chi_f\rangle = M|\chi_i\rangle / \sqrt{\langle \chi_i | M^\dagger M | \chi_i \rangle}$. Consequently, the entanglement power is given by

$$\mathcal{E}(E, \theta) = 1 - \int \frac{d\Omega_1}{4\pi} \frac{d\Omega_2}{4\pi} \text{Tr}[\rho_1^2], \quad (1)$$

where $\rho_1 = \text{Tr}_2(|\chi_f\rangle\langle\chi_f|)$ is the reduced density matrix for one proton, and the integral runs over all spin orientations.

The concurrence \mathcal{C} quantifies the entanglement of a two-qubit mixed state ρ . It is defined as

$$\mathcal{C}(\rho) = \max\{0, \lambda_1 - \lambda_2 - \lambda_3 - \lambda_4\}, \quad (2)$$

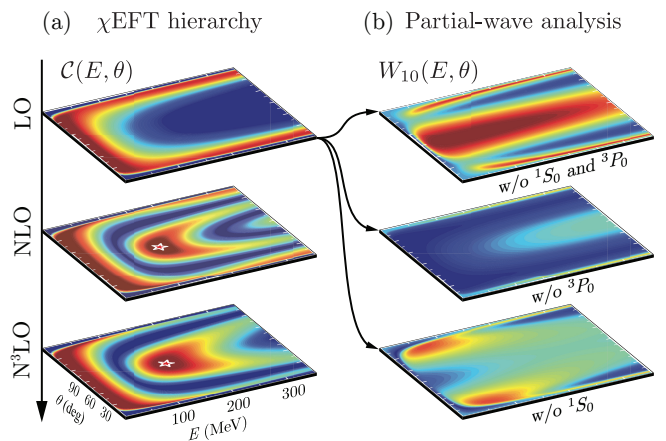


FIG. 2. (a) Concurrence \mathcal{C} calculated using chiral EFT at different orders. (b) Partial-wave decomposition of the Bell-triplet weight W_{10} at LO in chiral EFT. The three panels, from top to bottom, respectively show the results excluding the contributions from 1S_0 and 3P_0 components.

where $\{\lambda_i\}$ are the square roots of the eigenvalues of $R = \rho(\sigma_y \otimes \sigma_y) \rho^* (\sigma_y \otimes \sigma_y)$ in descending order [58, 59]. This measure ranges from 0 to 1, where 0 indicates an unentangled (separable) state and 1 corresponds to a maximally entangled state. For instance, all four Bell states yield $\mathcal{C} = 1$, confirming their maximal entanglement. As an experimentally accessible measure, concurrence is widely used as a genuine entanglement quantifier for two qubits [59].

Emergence of the entangled spin-triplet state—The entanglement power extracted from the Nijmegen PWA93 database (including Coulomb effects) is shown in Fig. 1(a). It exhibits a symmetric profile at the scattering angle $\theta = 90^\circ$, reflecting the indistinguishability of the two protons. Two pronounced enhancements are observed: one at low laboratory energies ($E < 10 \text{ MeV}$) and another around $(E, \theta) = (151 \text{ MeV}, 90^\circ)$, hereafter denoted as (E_\odot, θ_\odot) . These regions correspond to kinetic conditions that favor strong spin entanglement. The well-known low-energy enhancement originates from the 1S_0 partial-wave scattering, which generates the antisymmetric singlet state $|\Psi^-\rangle = (|\uparrow\downarrow\rangle - |\downarrow\uparrow\rangle) / \sqrt{2}$ [47, 60], long recognized as the essential configuration for nuclear Bell tests with proton singlet pairs [40, 41]. In sharp contrast, the distinct peak at (E_\odot, θ_\odot) reveals a previously unexplored regime where the scattering process gives rise to a strongly entangled spin-triplet state.

While the concept of entanglement power has garnered theoretical interest in nuclear physics [42–45], its direct experimental determination remains challenging. Given this limitation, we adopt concurrence \mathcal{C} as a more practical and experimentally accessible measure of spin entanglement. The concurrence map for a completely unpolarized initial state, Fig. 1(b), closely mirrors the entanglement-power landscape and reaches $\mathcal{C} = 0.977$ at (E_\odot, θ_\odot) . At this kinematic point, the reconstructed final-state density matrix is dominated by a single Bell-

triplet component,

$$\rho_f = a_1|\Psi^+\rangle\langle\Psi^+| + a_2|\Phi^-\rangle\langle\Phi^-| + a_3|\Psi^-\rangle\langle\Psi^-|, \quad (3)$$

with $a_1 = 0.988$, $a_2 = 0.009$, and $a_3 = 0.003$. Here $|\Psi^\pm\rangle = (|\uparrow\downarrow\rangle \pm |\downarrow\uparrow\rangle)/\sqrt{2}$ and $|\Phi^\pm\rangle = (|\uparrow\uparrow\rangle \pm |\downarrow\downarrow\rangle)/\sqrt{2}$ are the Bell basis states. To an excellent approximation, pp scattering in the vicinity of (E_\odot, θ_\odot) produces the pure Bell-triplet state $|\Psi^+\rangle$, providing a high-quality triplet source for further Bell tests and related applications (see Supplemental Material [61] for additional discussion).

Nature of the Bell-triplet state—To uncover the origin of the Bell-triplet window, we compute the concurrence using chiral EFT interactions from leading order (LO) up to N^3 LO [54], with Coulomb effects incorporated as in Refs. [47, 55]. Along $\theta = 90^\circ$, Fig. 2(a) shows that realistic interactions beyond LO reproduce the pronounced concurrence peak near $E_{\text{lab}} \simeq 151$ MeV, while LO largely misses it. As demonstrated below, the Bell-triplet window is actually a delicate consequence of the interplay between two ingredients: (i) the phase-shift pattern, through the resulting partial-wave balance, which largely fixes the energy where such a window can occur; and (ii) a microscopic spin-mixing mechanism that drives the outgoing state toward an almost pure triplet.

Indeed, the concurrence enhancement requires the dominant 1S_0 and 3P_0 contributions to be reduced so that other amplitudes can interfere coherently. We illustrate this by evaluating the Bell-triplet weight $W_{10} = \text{Tr}(\rho_f |\Psi^+\rangle\langle\Psi^+|)$ at LO while selectively excluding the 1S_0 and/or 3P_0 components. As shown in Fig. 2(b), removing these channels opens a broad triplet-favored region near $\theta = 90^\circ$, consistent with the interpretation that the phase shifts primarily determine where the window can appear.

The physics origin of the near-pure Bell triplet, however, is largely due to the tensor interaction. We therefore scale the tensor component of the N^3 LO chiral potential by c_T (i.e., $V_T \rightarrow c_T V_T$) and recompute the entanglement measures. Figure 3 shows that reducing c_T rapidly quenches the concurrence peak, while restoring the tensor strength recovers it; the same trend is seen for both \mathcal{C} and W_{10} at (E_\odot, θ_\odot) . This sensitivity has a clear operator-level origin: among the leading spin structures, the tensor operator $S_{12} = 3(\boldsymbol{\sigma}_1 \cdot \hat{\mathbf{r}})(\boldsymbol{\sigma}_2 \cdot \hat{\mathbf{r}}) - \boldsymbol{\sigma}_1 \cdot \boldsymbol{\sigma}_2$ mixes different magnetic components and efficiently transfers amplitude into the $m_s = 0$ triplet sector, thereby enhancing the $|\Psi^+\rangle$ component. Spin-orbit terms can induce analogous mixing, but their impact is typically subleading for the χ EFT interactions. Indeed, as demonstrated in the Supplemental Material [61], removing the tensor component precludes the emergence of a near-pure Bell triplet across the Argonne AV family [48, 62], although in that case the spin-orbit contribution can also be non-negligible. More broadly, this pronounced dependence suggests that precision measurements of spin entanglement could provide a direct and complementary constraint on the nuclear tensor and spin-orbit interaction.

Bell-state transition operator and quantum gate—The Bell-triplet dominance around (E_\odot, θ_\odot) is accompanied

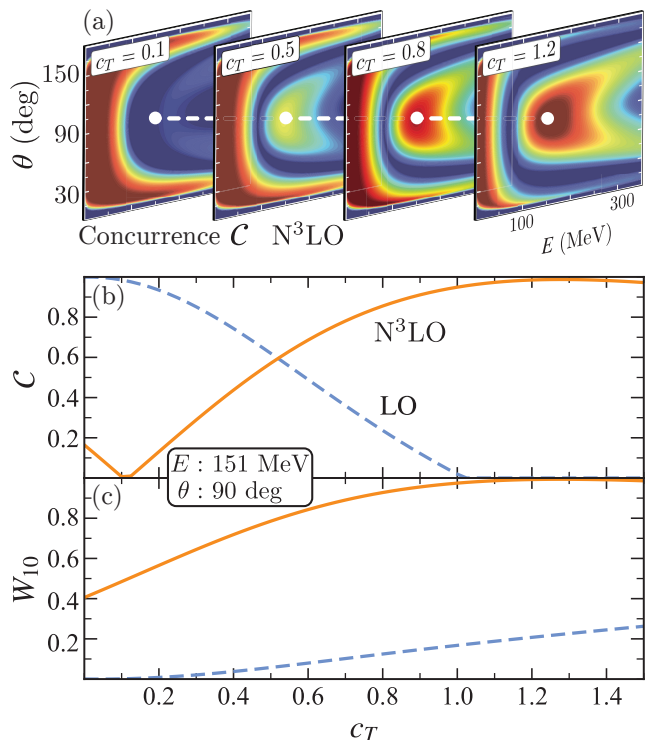


FIG. 3. (a) Concurrence \mathcal{C} calculated using the N^3 LO chiral EFT interaction with the tensor strength c_T varied. (b) Concurrence \mathcal{C} and (c) Bell-triplet weight W_{10} at $(E, \theta) = (151 \text{ MeV}, 90^\circ)$, calculated using both LO and N^3 LO chiral EFT interactions, plotted as a function of c_T .

by a remarkably simple structure at the amplitude level. In the Bell basis, the spin-dependent scattering amplitude is dominated by a single matrix element,

$$M(E_\odot, \theta_\odot) \simeq (-3.845 - i0.058) |\Psi^+\rangle\langle\Phi^-|, \quad (4)$$

with all other Bell-basis components smaller by more than one order of magnitude. Consequently, for any incoming two-proton state ρ_i with nonzero overlap with $|\Phi^-\rangle$,

$$\rho_f \propto M \rho_i M^\dagger \Rightarrow \rho_f \simeq |\Psi^+\rangle\langle\Psi^+|, \quad (5)$$

showing that pp scattering near (E_\odot, θ_\odot) coherently converts the $|\Phi^-\rangle$ component of the input into the Bell triplet.

In quantum-information terms, M realizes a native Bell-basis transition operation—a fixed entangling gate (up to local phases and post-selection) analogous to a Hadamard-plus-CNOT sequence in the computational basis [2]. This behavior contrasts with the low-energy regime ($E \lesssim 10$ MeV), where $M \propto |\Psi^-\rangle\langle\Psi^-|$ acts as an effective Bell-singlet projector. The evolution from projective to transition-operator-like behavior as the energy increases reveals that the nuclear scattering amplitude can function as a physically realized spin-entanglement processor, with the strong interaction providing the underlying mechanism for Bell-state manipulation. By effectively implementing a native Bell mea-

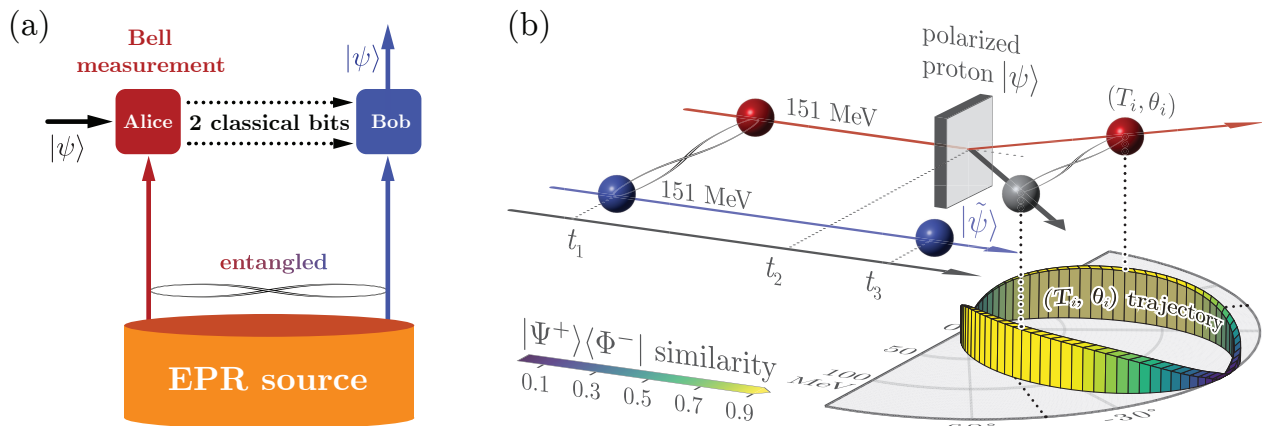


FIG. 4. (a) Standard quantum teleportation protocol using shared entanglement and Bell measurement. (b) Proposed proton spin teleportation at 151 MeV. Scattering near 90° (t_2) acts as a nuclear-force-driven Bell measurement, transferring the target spin state $|\psi\rangle$ —up to an inversion of the quantization axis—to the remote proton (t_3). The pie plot shows the kinematically allowed (T_i, θ_i) locus (laboratory kinetic energy and scattering angle) for a scattered proton; the histogram height and color encode the similarity \mathcal{S} [63] between the scattering amplitude M and the Bell transition operator $|\Psi^+\rangle\langle\Phi^-|$ (PWA93), indicating a broad angular range where the transition is effective (see Supplemental Material [61] for additional discussion).

surement through this transition mechanism, the pp scattering provides the critical physical resource required for quantum spin teleportation.

Spin teleportation—Quantum teleportation is well established in photonic and atomic platforms [64, 65], but it has not been demonstrated in MeV-scale nuclear reactions, despite early proposals based on standard nuclear scattering and polarization techniques [66, 67]. Bridging this gap would extend quantum information science into the femtometer domain and ultrafast dynamics governed by the strong interaction, with reduced exposure to external environmental noise. Moreover, it could also provide a pathway to map nuclear states onto accessible platforms, unlocking new avenues for probing nuclear structure via quantum state tomography.

While the standard protocol requires an entangled source, a Bell measurement, and classical communication as shown in Fig. 4(a), the nuclear environment presents unique opportunities and challenges. Entangled proton pairs can be generated through elastic pp scattering [40], charge-exchange reactions like $p(d, {}^2\text{He})n$ [41], and $2p$ decay of ${}^6\text{Be}$ [68, 69]. This makes the entangled resource experimentally accessible with standard beam/target and polarimetry techniques, without relying on charge-exchange reactions or rare decay sources; however, the strong interaction precludes the external quantum gates required for standard Bell measurements. To overcome this, we propose harnessing the intrinsic scattering dynamics. The pp scattering amplitude offers two avenues: the low-energy Bell singlet projector $M \propto |\Psi^-\rangle\langle\Psi^-|$ ($E < 10$ MeV), and the newly identified Bell-state transition operator, $M \propto |\Psi^+\rangle\langle\Phi^-|$, emerging around (E_\odot, θ_\odot) . Below, we focus on the second avenue; the low-energy singlet-based scheme is detailed in the Supplemental Material [61].

A schematic is shown in Fig. 4(b). Because all participants are protons (identical fermions), we use the in-

dices and colors in Fig. 4(b) to label *spatially separated modes* (arms/trajectories) rather than intrinsic particle identity; in the postselected subspace with one proton in each mode, the spin space is isomorphic to that of three distinguishable qubits. At time t_1 , an entangled Bell-singlet pair (red/blue) can be produced by the $p(d, {}^2\text{He})n$ reaction [41] or other established mechanisms discussed above—and split into two arms: a high-energy proton (red, mode 2) tuned to $E \simeq 151$ MeV and a remote partner (blue, mode 3). The proton in mode 2 then scatters elastically from a polarized proton target (gray, mode 1) prepared in the state $|\psi\rangle$. In the Bell-triplet window ($E \simeq 151$ MeV and $\theta \simeq 90^\circ$), the spin-dependent scattering amplitude is well approximated by a Bell-state transition, $M \propto |\Psi^+\rangle\langle\Phi^-|$, which transfers the target spin information to the remote proton. We postselect coincidence events in which the two outgoing protons populate two detector arms around $\pm 45^\circ$ in the laboratory frame, thereby defining the two-qubit output modes. Consequently, at t_3 , the blue proton carries state $|\tilde{\psi}\rangle$, which reproduces $|\psi\rangle$ up to a quantization axis inversion (i.e., a fixed, correctable single-qubit operation). The polarization of the blue proton can then be analyzed with standard polarimeters and compared to the known target polarization; such an agreement is a necessary condition for the success of proton spin teleportation. As detailed in the Supplemental Material [61], this protocol extends naturally from pure to mixed states.

Central to this scheme is the dynamical emergence of the Bell-state transition operator $|\Psi^+\rangle\langle\Phi^-|$ near (E_\odot, θ_\odot) . We quantify this by calculating the similarity between the physical scattering amplitude M (from PWA93) and the transition operator $|\Psi^+\rangle\langle\Phi^-|$ using the normalized trace metric $\mathcal{S}(E, \theta) = |\text{Tr}(M^\dagger(E, \theta) |\Psi^+\rangle\langle\Phi^-|)| / \sqrt{\text{Tr}(M^\dagger(E, \theta) M(E, \theta))}$ [63]. As shown in Fig. 4(b) and Supplemental Material [61], a high-similarity “island” appears around (E_\odot, θ_\odot) , indi-

cating that the nuclear force naturally generates an amplitude close to the required gate over a broad kinematic window.

Regarding the classical communication required for teleportation, it is naturally built into the scattering-based implementation. The kinematic postselection makes the reaction an intrinsically probabilistic filter, so that the usual two-bit message (required to identify one of four Bell outcomes) is effectively reduced to a single bit: whether a valid event occurred at the prescribed kinematics. This “event-ready” signal is provided by coincident detection of the outgoing protons, which both heralds successful operation and supplies the required classical communication while explicitly reflecting the probabilistic character of the interaction.

Summary—Our study exemplifies how concepts from quantum information science can provide new perspectives on nucleon-nucleon scattering and nuclear force, long regarded as well understood. Specifically, we reveal a pronounced region around $(E_{\odot}, \theta_{\odot}) = (151 \text{ MeV}, 90^{\circ})$ in pp scattering that is highly conducive to spin entanglement generation. Calculations using the Nijmegen PWA93 database and chiral EFT interactions demonstrate that the scattering output at this kinematic point forms a nearly pure Bell-triplet state $|\Psi^+\rangle$ for all chiral orders beyond LO. We identify the tensor force as the key

dynamical driver responsible for generating this unique entanglement structure. Analysis of the underlying spin amplitude further reveals that it acts predominantly as a transition operator of the form $\propto |\Psi^+\rangle \langle \Phi^-|$. Building on this finding, we propose a protocol for proton spin teleportation where the scattering amplitude itself serves as a natural Bell measurement. The realization of such spin teleportation via the strong interaction would extend the reach of quantum information protocols into the femtometer regime, offering a novel method for the faithful transfer and manipulation of nuclear quantum states.

Acknowledgments—We thank Dean Lee, Mart Rentmeester and Kentaro Yako for helpful communications and discussions. This work is supported by the National Natural Science Foundation of China (Grants No. 12347106, No. 12547102, No. 12447122, and No. 12375122), the National Key Research and Development Program of China (MOST 2023YFA1606404 and MOST 2022YFA1602303), and the China Postdoctoral Science Foundation (Grant No. 2024M760489).

Note added—This work on spin teleportation was initiated in October 2025. The main findings were presented by D.B. on behalf of the collaboration at the Solenoidal Spectrometer Workshop 2025 on December 9; slides are available at [70].

-
- [1] R. Horodecki, P. Horodecki, M. Horodecki, and K. Horodecki, Quantum entanglement, *Rev. Mod. Phys.* **81**, 865 (2009).
- [2] M. Nielsen and I. L. Chuang, *Quantum Computation and Quantum Information: 10th Anniversary Edition* (Cambridge University Press, 2010).
- [3] J. I. Cirac and P. Zoller, Quantum computations with cold trapped ions, *Phys. Rev. Lett.* **74**, 4091 (1995).
- [4] C. Monroe, D. M. Meekhof, B. E. King, W. M. Itano, and D. J. Wineland, Demonstration of a fundamental quantum logic gate, *Phys. Rev. Lett.* **75**, 4714 (1995).
- [5] K. Mølmer and A. Sørensen, Multiparticle entanglement of hot trapped ions, *Phys. Rev. Lett.* **82**, 1835–1838 (1999).
- [6] A. Sørensen, L.-M. Duan, J. I. Cirac, and P. Zoller, Many-particle entanglement with bose–einstein condensates, *Nature* **409**, 63–66 (2001).
- [7] Y. S. Athreya, S. Kannan, X. T. Yan, R. J. Lewis-Swan, K. V. Kheruntsyan, A. G. Truscott, and S. S. Hodgman, Bell correlations between momentum-entangled pairs of $^4\text{He}^*$ atoms, *Nat. Commun.* (2026).
- [8] B. Yang, H. Sun, C.-J. Huang, H.-Y. Wang, Y.-J. Deng, H.-N. Dai, Z.-S. Yuan, and J.-W. Pan, Cooling and entangling ultracold atoms in optical lattices, *Science* **369**, 550–553 (2020).
- [9] M. H. Devoret, J. M. Martinis, D. Esteve, and J. Clarke, Resonant activation from the zero-voltage state of a current-biased Josephson junction, *Phys. Rev. Lett.* **53**, 1260 (1984).
- [10] J. M. Martinis, M. H. Devoret, and J. Clarke, Energy-level quantization in the zero-voltage state of a current-biased Josephson junction, *Phys. Rev. Lett.* **55**, 1543 (1985).
- [11] M. H. Devoret, J. M. Martinis, and J. Clarke, Measurements of macroscopic quantum tunneling out of the zero-voltage state of a current-biased Josephson junction, *Phys. Rev. Lett.* **55**, 1908 (1985).
- [12] The BESIII Collaboration, Polarization and entanglement in baryon–antibaryon pair production in electron–positron annihilation, *Nat. Phys.* **15**, 631 (2019).
- [13] The BESIII Collaboration, Probing CP symmetry and weak phases with entangled double-strange baryons, *Nature* **606**, 64 (2022).
- [14] The ATLAS Collaboration, Observation of quantum entanglement with top quarks at the ATLAS detector, *Nature* **633**, 542 (2024).
- [15] J. H. Chen *et al.*, Properties of the QCD matter: review of selected results from the relativistic heavy ion collider beam energy scan (RHIC BES) program, *Nucl. Sci. Tech.* **35**, 214 (2024).
- [16] The BESIII Collaboration, Test of local realism via entangled $\Lambda\bar{\Lambda}$ system, *Nat. Commun.* **16**, 4948 (2025).
- [17] J. Aziz and R. Howl, Classical theories of gravity produce entanglement, *Nature* **646**, 813 (2025).
- [18] M. Hentschinski, D. E. Kharzeev, K. Kutak, and Z. Tu, Probing the onset of maximal entanglement inside the proton in diffractive deep inelastic scattering, *Phys. Rev. Lett.* **131**, 241901 (2023).
- [19] Y. Guo, X. Liu, F. Yuan, and H. X. Zhu, Long-range azimuthal correlation, entanglement, and bell inequality violation by spinning gluons at the large hadron collider, *Research* **8**, 0552 (2025).
- [20] K. Ehatäht, M. Fabbrichesi, L. Marzola, and C. Veelken, Probing entanglement and testing bell inequality viola-

- tion with $e^+e^- \rightarrow \tau^+\tau^-$ at belle ii, *Phys. Rev. D* **109**, 032005 (2024).
- [21] Y. Afik, Y. Kats, J. R. Muñoz de Nova, A. Soffer, and D. Uzan, Entanglement and bell nonlocality with bottom-quark pairs at hadron colliders, *Phys. Rev. D* **111**, L111902 (2025).
- [22] S. R. Beane, D. B. Kaplan, N. Klco, and M. J. Savage, Entanglement suppression and emergent symmetries of strong interactions, *Phys. Rev. Lett.* **122**, 102001 (2019).
- [23] C. W. Johnson and O. C. Gorton, Proton–neutron entanglement in the nuclear shell model, *J. Phys. G* **50**, 045110 (2023).
- [24] C. E. P. Robin, M. J. Savage, and N. Pillet, Entanglement rearrangement in self-consistent nuclear structure calculations, *Phys. Rev. C* **103**, 034325 (2021).
- [25] D. Bai and Z. Ren, Entanglement generation in few-nucleon scattering, *Phys. Rev. C* **106**, 064005 (2022).
- [26] T. Kirchner, W. Elkamhawy, and H.-W. Hammer, Entanglement in Few-Nucleon Scattering Events, *Few Body Syst.* **65**, 29 (2024).
- [27] Y. G. Ma, New type of double-slit interference experiment at Fermi scale, *Nucl. Sci. Tech.* **34**, 16 (2023).
- [28] C. E. P. Robin and M. J. Savage, Quantum complexity fluctuations from nuclear and hypernuclear forces, [arXiv:2405.10268](https://arxiv.org/abs/2405.10268) (2024).
- [29] Y. Qiang, J. C. Pei, and K. Godbey, Quantum entanglement in nuclear fission, *Phys. Lett. B* **861**, 139248 (2025).
- [30] H. Y. Shang, Y. Qiang, and J. C. Pei, Energy partition between entangled fission fragments, *Nucl. Sci. Tech.* **36**, 211 (2025).
- [31] C. E. P. Robin and M. J. Savage, Anti-flatness and non-local magic in two-particle scattering processes, [arXiv:2510.23426](https://arxiv.org/abs/2510.23426) (2025).
- [32] C. Pacheco and N. R. Shah, Gedanken experiments of entanglement in particle physics: Interactions, operators and bell inequalities in flavor space, [arXiv:2512.23855](https://arxiv.org/abs/2512.23855) (2025).
- [33] D. K. Shin, B. M. Henson, S. S. Hodgman, T. Wasak, J. Chwedeńczuk, and A. G. Truscott, Bell correlations between spatially separated pairs of atoms, *Nat. Commun.* **10**, 4447 (2019).
- [34] W. Rosenfeld, D. Burchardt, R. Garthoff, K. Redeker, N. Ortegel, M. Rau, and H. Weinfurter, Event-ready bell test using entangled atoms simultaneously closing detection and locality loopholes, *Phys. Rev. Lett.* **119**, 010402 (2017).
- [35] J. Gu, S.-J. Lin, D. Y. Shao, L.-T. Wang, and S.-X. Yang, Decoherence in high energy collisions as renormalization group flow, [arXiv:2510.13951](https://arxiv.org/abs/2510.13951) (2025).
- [36] S.-J. Lin, M.-J. Liu, D. Y. Shao, and S.-Y. Wei, Spin correlations and bell nonlocality in $\Lambda\bar{\Lambda}$ pair production from e^+e^- collisions with a thrust cut, *JHEP* **2025** (11), 082.
- [37] D. Bai, Toward experimental determination of spin entanglement of nucleon pairs, *Phys. Rev. C* **109**, 034001 (2024).
- [38] E. Epelbaum, H.-W. Hammer, and U.-G. Meissner, Modern theory of nuclear forces, *Rev. Mod. Phys.* **81**, 1773 (2009).
- [39] R. Machleidt and D. R. Entem, Chiral effective field theory and nuclear forces, *Phys. Rept.* **503**, 1 (2011).
- [40] M. Laméhi-Rachti and W. Mittig, Quantum mechanics and hidden variables: A test of Bell’s inequality by the measurement of the spin correlation in low-energy proton–proton scattering, *Phys. Rev. D* **14**, 2543 (1976).
- [41] H. Sakai, T. Saito, T. Ikeda, K. Itoh, T. Kawabata, H. Kuboki, Y. Maeda, N. Matsui, C. Rangacharyulu, M. Sasano, Y. Satou, K. Sekiguchi, K. Suda, A. Tamii, T. Uesaka, and K. Yako, Spin correlations of strongly interacting massive fermion pairs as a test of Bell’s inequality, *Phys. Rev. Lett.* **97**, 150405 (2006).
- [42] D. Bai, Spin entanglement in neutron–proton scattering, *Phys. Lett. B* **845**, 138162 (2023).
- [43] G. A. Miller, Entanglement maximization in low-energy neutron–proton scattering, *Phys. Rev. C* **108**, L031002 (2023).
- [44] A. L. Cavallin, O. Thim, and C. Forssén, Entanglement and accidental symmetries in the nucleon–nucleon system, [arXiv:2510.09466](https://arxiv.org/abs/2510.09466) (2025).
- [45] H. Witała, J. Golak, and R. Skibiński, Searching for entanglement in final polarization states of the neutron–proton scattering, [arXiv:2505.14401](https://arxiv.org/abs/2505.14401) (2025).
- [46] H. Witała, Investigation of entanglement in pure final polarization states from neutron–deuteron elastic scattering and exclusive deuteron breakup, [arXiv:2510.10664](https://arxiv.org/abs/2510.10664) (2025).
- [47] V. G. J. Stoks, R. A. M. Klomp, M. C. M. Rentmeester, and J. J. de Swart, Partial-wave analysis of all nucleon–nucleon scattering data below 350 MeV, *Phys. Rev. C* **48**, 792 (1993).
- [48] R. B. Wiringa, V. G. J. Stoks, and R. Schiavilla, Accurate nucleon–nucleon potential with charge-independence breaking, *Phys. Rev. C* **51**, 38 (1995).
- [49] R. Machleidt, High-precision, charge-dependent Bonn nucleon–nucleon potential, *Phys. Rev. C* **63**, 024001 (2001).
- [50] E. Epelbaum, H. Krebs, and U. G. Meißner, Precision nucleon–nucleon potential at fifth order in the chiral expansion, *Phys. Rev. Lett.* **115**, 122301 (2015).
- [51] D. R. Entem, R. Machleidt, and Y. Nosyk, High-quality two-nucleon potentials up to fifth order of the chiral expansion, *Phys. Rev. C* **96**, 024004 (2017).
- [52] C. H. Bennett, G. Brassard, C. Crépeau, R. Jozsa, A. Peres, and W. K. Wootters, Teleporting an unknown quantum state via dual classical and einstein-podolsky-rosen channels, *Phys. Rev. Lett.* **70**, 1895 (1993).
- [53] The Nijmegen group, NN-Online: Nucleon-Nucleon Scattering Data and Phase Shifts, <https://nn-online.org/> (2025), accessed: 2025-03-07.
- [54] S. K. Saha, D. R. Entem, R. Machleidt, and Y. Nosyk, Local position-space two-nucleon potentials from leading to fourth order of chiral effective field theory, *Phys. Rev. C* **107**, 034002 (2023).
- [55] J. R. Bergervoet, P. C. van Campen, W. A. van der Sanden, and J. J. de Swart, Phase shift analysis of 0–30 MeV pp scattering data, *Phys. Rev. C* **38**, 15 (1988).
- [56] P. Zanardi, C. Zalka, and L. Faoro, Entangling power of quantum evolutions, *Phys. Rev. A* **62**, 030301(R) (2000).
- [57] A. Datta, S. T. Flammia, and C. M. Caves, Entanglement and the power of one qubit, *Phys. Rev. A* **72**, 042316 (2005).
- [58] S. A. Hill and W. K. Wootters, Entanglement of a pair of quantum bits, *Phys. Rev. Lett.* **78**, 5022 (1997).
- [59] W. K. Wootters, Entanglement of formation of an arbitrary state of two qubits, *Phys. Rev. Lett.* **80**, 2245 (1998).
- [60] W. Glöckle, *The Quantum Mechanical Few-Body Problem* (Springer-Verlag, Berlin, Heidelberg, 1983).
- [61] See Supplemental Material at [URL inserted by publisher] for details on the Bell measurement and quantum

teleportation in nuclear physics.

- [62] R. B. Wiringa and S. C. Pieper, Evolution of nuclear spectra with nuclear forces, [Phys. Rev. Lett. **89**, 182501 \(2002\)](#).
- [63] J. Watrous, *The Theory of Quantum Information* (Cambridge University Press, 2018).
- [64] S. Pirandola, J. Eisert, C. Weedbrook, A. Furusawa, and S. L. Braunstein, Advances in quantum teleportation, [Nature Photon. **9**, 641 \(2015\)](#).
- [65] X.-M. Hu, Y. Guo, B.-H. Liu, C.-F. Li, and G.-C. Guo, Progress in quantum teleportation, [Nat. Rev. Phys. **5**, 339 \(2023\)](#).
- [66] B. F. Kostenko, V. D. Kuznetsov, D. V. Kamanin, and M. B. Miller, Possibility for teleportation of nuclei, [arXiv:quant-ph/0012133 \(2000\)](#), This proposal operates at 20–50 MeV, where well-defined Bell operators do not naturally emerge. In contrast, our scheme exploits the regimes $E < 10$ MeV and $E \approx 151$ MeV, where such operators arise from the scattering dynamics.
- [67] V. V. Ivanov, B. F. Kostenko, V. D. Kuznetsov, M. B. Miller, and A. V. Sermyagin, Quantum teleportation of nuclear matter and its investigation, *Particles and Nuclei, Letters* **1**[116], 96 (2003), The same remark made regarding Ref. [52] applies to this reference.
- [68] S. M. Wang and W. Nazarewicz, Fermion Pair Dynamics in Open Quantum Systems, [Phys. Rev. Lett. **126**, 142501 \(2021\)](#).
- [69] T. Oishi, Spin correlation in two-proton emission from ${}^6\text{Be}$, [Phys. Lett.s B **862**, 139361 \(2025\)](#).
- [70] D. Bai, Spin-state teleportation at mev energies via entanglement generation and manipulation between protons, [Solenoidal Spectrometer Workshop 2025](#) .
- [71] R. Horodecki, P. Horodecki, and M. Horodecki, Violating Bell inequality by mixed spin-1/2 states: Necessary and sufficient condition, [Phys. Lett. A **200**, 340 \(1995\)](#).
- [72] N. Brunner, D. Cavalcanti, S. Pironio, V. Scarani, and S. Wehner, Bell nonlocality, [Rev. Mod. Phys. **86**, 419 \(2014\)](#).
- [73] J. F. Clauser, M. A. Horne, A. Shimony, and R. A. Holt, Proposed experiment to test local hidden-variable theories, [Phys. Rev. Lett. **23**, 880 \(1969\)](#).

Supplemental Material for “Spin Teleportation via Bell-Triplet States Emergent from Proton-Proton Scattering”

This Supplemental Material contains:

- **Triplet source and feasibility estimates:** an order-of-magnitude production-rate estimate for near-pure Bell-triplet proton pairs from unpolarized pp scattering at $(E_{\odot}, \theta_{\odot})$, based on the differential cross section and typical beam/target/acceptance parameters.
- **Nuclear Bell tests in the triplet regime:** an assessment of CHSH-inequality violations using the Horodecki criterion, together with the corresponding spin-correlation function $F(\mathbf{n}_1, \mathbf{n}_2)$ evaluated from the PWA93 spin-density matrix.
- **Realistic interactions and operator hierarchy:** a comparative study of the Argonne AV family (AV18, AV8', AV6', AV4') demonstrating that the tensor force is the essential seed for the Bell-triplet window while the spin-orbit term acts as a key amplifier, with higher-order operators providing only minor corrections to W_{10} .
- **Teleportation preliminaries:** a brief, self-contained review of the standard qubit-teleportation protocol (notation and key steps) to establish the framework used in the main text.
- **Proton spin teleportation at $(151 \text{ MeV}, 90^\circ)$:** a step-by-step derivation showing that the scattering operator acts as a Bell-state transition, $M \propto |\Psi^+\rangle\langle\Phi^-|$.
- **Low-energy proton spin teleportation ($E < 10 \text{ MeV}$):** a complementary derivation for the S -wave-dominated regime where the scattering amplitude reduces to a Bell-singlet projector, $M \propto |\Psi^-\rangle\langle\Psi^-|$.
- **Supplemental figures:** additional plots supporting the feasibility analysis and the teleportation derivations.

I. Triplet sources and nuclear Bell tests

The identification of the Bell-triplet state at $(E_{\odot}, \theta_{\odot})$ establishes unpolarized pp scattering as a promising source for proton triplet pairs. The feasibility of large-scale production is supported by the sizable differential cross section of 3.72 mb/sr at this kinematic point. Under typical experimental conditions with a solid-angle acceptance of $\Delta\Omega = 0.01$ sr, a proton beam current of 100 nA, and a 0.10 cm thick liquid hydrogen target, the estimated production rate of these triplet pairs reaches $\sim 10^5$ s $^{-1}$.

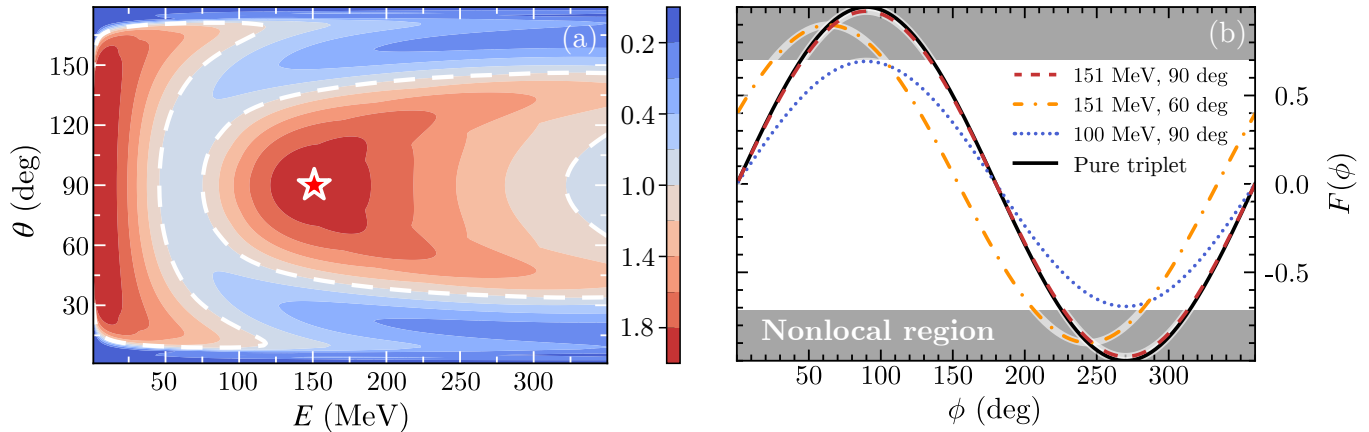


FIG. S1. (a) Horodecki function $H(\rho_f)$ derived from the Nijmegen PWA93 database. (b) Spin correlation function $F(\phi) = \text{Tr}[(\boldsymbol{\sigma}_1 \cdot \mathbf{n}_1) \otimes (\boldsymbol{\sigma}_2 \cdot \mathbf{n}_2)\rho_f]$ computed from the same database. The measurement geometry is defined by a fixed analyzer along $\mathbf{n}_1 = (1, 0, 0)$ and a second analyzer rotating in the x - z plane as $\mathbf{n}_2 = (\sin \phi, 0, \cos \phi)$.

The availability of proton triplet pairs opens new avenues for *nuclear Bell tests*, which thus far have relied exclusively on proton singlet pairs. To assess the feasibility of Bell-inequality violations in the triplet regime, we adopt the Horodecki criterion [71, 72], which identifies the kinematic regions where the Clauser–Horne–Shimony–Holt (CHSH) inequality [73] can be violated. Figure S1(a) shows a contour map of the Horodecki function $H(\rho_f) = u_1 + u_2$, where $u_{1,2}$ are the two largest eigenvalues of the matrix $U = \tilde{U}^T \tilde{U}$, with correlation-tensor elements $\tilde{U}_{ij} = \text{Tr}(\rho_f \sigma_i \otimes \sigma_j)$. A violation of the CHSH inequality is signaled by $H(\rho_f) > 1$. The white dashed curve, representing the contour $H(\rho_f) = 1$, separates the CHSH-violating (red) and non-violating (blue) domains. The pronounced maximum at $(E_{\odot}, \theta_{\odot})$, marked by a red pentagram, together with the surrounding dark-red area, delineates a broad kinematic region suitable for nuclear Bell tests using triplet proton pairs.

The spin correlation function $F(\mathbf{n}_1, \mathbf{n}_2) = \text{Tr}[(\boldsymbol{\sigma}_1 \cdot \mathbf{n}_1) \otimes (\boldsymbol{\sigma}_2 \cdot \mathbf{n}_2)\rho_f]$ is commonly measured in experimental tests of Bell inequalities. Using the spin density matrix obtained from the PWA93 database, we evaluate F under various conditions, as shown in Fig. S1(b). In the calculation, the first measurement axis is fixed along the x -axis, $\mathbf{n}_1 = (1, 0, 0)$, while the second axis is rotated by an angle ϕ in the x - z plane, $\mathbf{n}_2 = (\sin \phi, 0, \cos \phi)$. For comparison, the ideal pure triplet state $|\Psi^+\rangle$ yields $F_{\text{triplet}}(\phi) = \sin \phi$. The shaded regions correspond to $|F(\phi)| > 1/\sqrt{2}$, the threshold for Bell-inequality violation, signifying that the spin correlations are strong enough to confirm quantum entanglement. Remarkably, even without further purification, the outgoing proton pairs at (151 MeV, 90 $^\circ$) retain pronounced potential for Bell tests, requiring no fine tuning of beam energy or scattering angle.

II. Realistic interactions and the emergent Bell-triplet window

To test the robustness and microscopic origin of the emergent Bell-triplet window beyond χ EFT, we repeat the entanglement analysis with the Argonne AV family [48, 62], whose operator content can be truncated in a controlled manner. Specifically, as summarized in Table S1, AV4' retains only central spin-isospin operators (no tensor and no spin-orbit), AV6' adds the tensor operator but still omits spin-orbit terms, AV8' further includes spin-orbit operators, and AV18 contains the full operator structure.

TABLE S1. Bell-triplet weight W_{10} at $(E, \theta) = (151 \text{ MeV}, 90^\circ)$ and its maximum over the scanned kinematics for Argonne interactions with controlled operator content.

Potential	Operators	Tensor	Spin-orbit	$W_{10}(151 \text{ MeV}, 90^\circ)$	$\max W_{10}$
AV18	18 (full)	Yes	Yes	0.9885	0.9889
AV8'	8 (central + $\sigma \cdot \sigma$ + tensor + spin-orbit)	Yes	Yes	0.9882	0.9927
AV6'	6 (central + $\sigma \cdot \sigma$ + tensor)	Yes	No	0.4633	0.4633
AV4'	4 (central + $\sigma \cdot \sigma$)	No	No	0.0001	0.3331

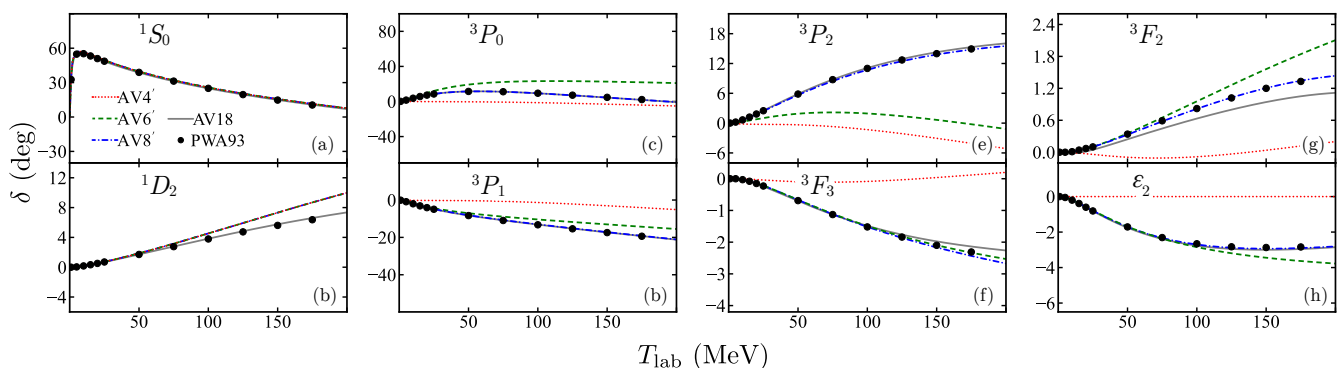


FIG. S2. Representative pp phase shifts obtained with AV4' (dotted), AV6' (dashed), AV8' (dash-dotted), and AV18 (solid), compared with Nijmegen PWA93 analysis (symbols).

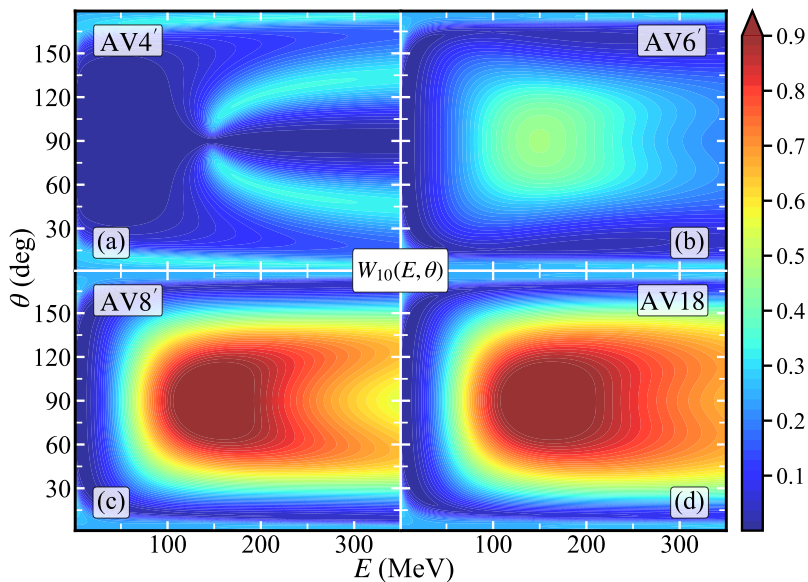


FIG. S3. Bell-triplet weight $W_{10}(E, \theta)$ computed with Argonne interactions. The entangled triplet window around (E_\odot, θ_\odot) is reproduced by interactions with a strong tensor sector (AV8', AV18), while it is absent without tensor terms (AV4') and strongly suppressed in truncated cases.

Although these interactions roughly reproduce the dominant low-energy trends of the pp phase shifts (Fig. S2), their entanglement responses differ qualitatively. Figure S3 shows that the near-pure Bell-triplet window around (E_\odot, θ_\odot)

appears only when a sufficiently strong tensor sector is present, and it disappears when tensor terms are removed (AV4').

The contrast between AV6' and AV8' isolates the impact of spin-orbit dynamics once the tensor force is present (see Fig. S3 and Table S1). With tensor but no spin-orbit, AV6' already produces a non-negligible population of the $m_s = 0$ triplet sector, leading to a localized enhancement of $W_{10}(E, \theta)$ around (150 MeV, 90°) in Fig. S3. However, the enhancement remains moderate ($W_{10} \simeq 0.46$ at the benchmark point) and does not develop into a near-unity window. When realistic spin-orbit operators are included (AV8'), the effect is amplified dramatically: W_{10} rises from ~ 0.46 to ~ 0.99 at (151 MeV, 90°). (For the χ EFT interaction considered in the main text, the corresponding spin-orbit enhancement is typically subleading relative to the tensor effect.) Microscopically, the tensor interaction provides the essential magnetic-substate mixing that feeds the $m_s = 0$ triplet channel, while the spin-orbit interaction reshapes the interference among the dominant partial waves in this energy range (notably the P waves), suppressing competing contributions and allowing the tensor-driven Bell-triplet channel to dominate.

A comparison between AV8' and AV18 further shows that the additional operator structures in AV18 (e.g., quadratic spin-orbit and charge-dependent terms) have only a minor impact on the Bell-triplet window and on W_{10} at the benchmark point: the window is essentially saturated once tensor and spin-orbit operators are included. Conversely, AV4' demonstrates that tensor dynamics are indispensable. Without the tensor operator S_{12} , W_{10} is essentially zero at $\theta = 90^\circ$ and never becomes large anywhere in the scan (Table S1), consistent with the absence of tensor-induced spin mixing.

Finally, at low energies ($E \lesssim 50$ MeV) all four potentials yield $W_{10} \approx 0$, reflecting the familiar 1S_0 singlet dominance in the pp channel enforced by the Pauli principle and S -wave scattering. Taken together, Table S1 and Figs. S3 and S2 establish a clear hierarchy for the dynamical origin of the Bell-triplet window: the tensor force provides the essential seed, the spin-orbit interaction acts as a powerful amplifier in the relevant kinematic window, and the remaining higher-order operator structures in AV18 play only a subleading role for W_{10} .

III. The standard quantum teleportation

Quantum teleportation is a fundamental protocol in quantum information science that enables the transfer of an unknown quantum state between distant parties using shared entanglement and classical communication [52]. Here we provide a self-contained introduction to the standard protocol, which contributes to the theoretical basis for the proton spin teleportation scheme discussed in the main text.

Consider two parties, Alice and Bob, who wish to transfer an unknown qubit state from Alice to Bob. The protocol involves three qubits: qubit 1 (the data qubit held by Alice carrying the unknown state), and qubits 2 and 3 (an entangled pair shared between Alice and Bob, with Alice holding qubit 2 and Bob holding qubit 3).

The unknown state to be teleported is

$$|\psi\rangle_1 = \alpha |0\rangle_1 + \beta |1\rangle_1, \quad (\text{S6})$$

where α and β are complex coefficients satisfying $|\alpha|^2 + |\beta|^2 = 1$. Alice and Bob share a maximally entangled Bell state, taken here to be

$$|\Psi^-\rangle_{23} = \frac{1}{\sqrt{2}} (|01\rangle_{23} - |10\rangle_{23}). \quad (\text{S7})$$

The four Bell states, which form an orthonormal basis for the two-qubit Hilbert space, are given by

$$\begin{aligned} |\Psi^\pm\rangle_{23} &= \frac{1}{\sqrt{2}} (|01\rangle_{23} \pm |10\rangle_{23}), \\ |\Phi^\pm\rangle_{23} &= \frac{1}{\sqrt{2}} (|00\rangle_{23} \pm |11\rangle_{23}). \end{aligned} \quad (\text{S8})$$

The initial state of the three-qubit system is the product state $|\psi\rangle_1 \otimes |\Psi^-\rangle_{23}$. Expanding this in terms of the Bell basis for qubits 1 and 2 yields

$$\begin{aligned} |\psi\rangle_1 \otimes |\Psi^-\rangle_{23} &= (\alpha |0\rangle_1 + \beta |1\rangle_1) \otimes \frac{1}{\sqrt{2}} (|01\rangle_{23} - |10\rangle_{23}) \\ &= \frac{1}{2} \left[|\Phi^+\rangle_{12} \otimes (\alpha |1\rangle_3 - \beta |0\rangle_3) + |\Phi^-\rangle_{12} \otimes (\alpha |1\rangle_3 + \beta |0\rangle_3) \right. \\ &\quad \left. + |\Psi^+\rangle_{12} \otimes (-\alpha |0\rangle_3 + \beta |1\rangle_3) + |\Psi^-\rangle_{12} \otimes (-\alpha |0\rangle_3 - \beta |1\rangle_3) \right]. \end{aligned} \quad (\text{S9})$$

Alice then performs a Bell measurement on qubits 1 and 2, projecting them onto one of the four Bell states with equal probability of 1/4. The measurement outcome, encoded by two classical bits, is transmitted to Bob. Depending on the result, Bob's qubit 3 is left in one of four states, each related to the original state $|\psi\rangle$ by a known unitary transformation:

$$\begin{aligned} |\Phi^+\rangle_{12} &: |\psi'\rangle_3 = \alpha |1\rangle_3 - \beta |0\rangle_3, \\ |\Phi^-\rangle_{12} &: |\psi'\rangle_3 = \alpha |1\rangle_3 + \beta |0\rangle_3, \\ |\Psi^+\rangle_{12} &: |\psi'\rangle_3 = -\alpha |0\rangle_3 + \beta |1\rangle_3, \\ |\Psi^-\rangle_{12} &: |\psi'\rangle_3 = -\alpha |0\rangle_3 - \beta |1\rangle_3. \end{aligned} \quad (\text{S10})$$

Upon receiving Alice's two classical bits, Bob applies the appropriate Pauli correction to recover the original state:

$$\begin{aligned} |\Phi^+\rangle_{12} &\Rightarrow ZX |\psi'\rangle_3 = \alpha |0\rangle_3 + \beta |1\rangle_3, \\ |\Phi^-\rangle_{12} &\Rightarrow X |\psi'\rangle_3 = \alpha |0\rangle_3 + \beta |1\rangle_3, \\ |\Psi^+\rangle_{12} &\Rightarrow Z |\psi'\rangle_3 = \alpha |0\rangle_3 + \beta |1\rangle_3, \\ |\Psi^-\rangle_{12} &\Rightarrow \mathbf{1} |\psi'\rangle_3 = \alpha |0\rangle_3 + \beta |1\rangle_3, \end{aligned} \quad (\text{S11})$$

where $X = \sigma_x$ and $Z = \sigma_z$ are the Pauli matrices. In all cases, the unknown quantum state $|\psi\rangle$ is faithfully transferred to Bob's qubit, completing the teleportation.

IV. Proton spin teleportation at $(E_{\odot}, \theta_{\odot}) = (151 \text{ MeV}, 90^{\circ})$

In this section, we provide a detailed step-by-step analysis of the proton spin teleportation protocol at the kinematic point $(E_{\odot}, \theta_{\odot}) = (151 \text{ MeV}, 90^{\circ})$, where the scattering amplitude acts as a Bell-state transition operator $M \propto |\Psi^+\rangle\langle\Phi^-|$.

Setup—The protocol involves three *spatially separated single-proton modes*, whose spin degrees of freedom serve as qubits. We label these modes by the same indices/colors as in Fig. 4(b):

- Mode 1 (gray): the polarized target proton carrying the unknown spin state $|\psi\rangle_1 = \alpha|0\rangle_1 + \beta|1\rangle_1$ to be teleported, where $|\alpha|^2 + |\beta|^2 = 1$.
- Mode 2 (red): one proton from an entangled pair, which will scatter with the target.
- Mode 3 (blue): the remote partner of the entangled pair, which will receive the teleported state.

Although all three particles are protons, the indices 1, 2, 3 refer to these modes (paths/arms) and are therefore operationally distinguishable. In the postselected subspace with one proton in each mode, the spin Hilbert space is equivalent to that of three distinguishable qubits; exchange antisymmetry is already encoded in the pp amplitude used to construct M . The entangled proton pair (protons 2 and 3) is prepared in the Bell-singlet state $|\Psi^-\rangle_{23}$ via, e.g., the $p(d, {}^2\text{He})n$ charge-exchange reaction, following the technique of Ref. [41]. The projectile deuteron energy is chosen such that the outgoing protons have a kinetic energy of approximately 151 MeV.

Spin state at t_1 —At time t_1 , after the entangled pair is produced and before the scattering with the polarized target, the three-proton spin state is the product

$$|\Psi(t_1)\rangle = |\psi\rangle_1 \otimes |\Psi^-\rangle_{23} = (\alpha|0\rangle_1 + \beta|1\rangle_1) \otimes \frac{1}{\sqrt{2}}(|01\rangle_{23} - |10\rangle_{23}). \quad (\text{S12})$$

To analyze the effect of the subsequent scattering, we expand this state in terms of the Bell basis for qubits 1 and 2:

$$|\Psi(t_1)\rangle = \frac{1}{2} \left[|\Phi^+\rangle_{12} \otimes (\alpha|1\rangle_3 - \beta|0\rangle_3) + |\Phi^-\rangle_{12} \otimes (\alpha|1\rangle_3 + \beta|0\rangle_3) \right. \\ \left. + |\Psi^+\rangle_{12} \otimes (-\alpha|0\rangle_3 + \beta|1\rangle_3) + |\Psi^-\rangle_{12} \otimes (-\alpha|0\rangle_3 - \beta|1\rangle_3) \right]. \quad (\text{S13})$$

This expansion reveals that each Bell-state component for qubits 1 and 2 is correlated with a distinct state of qubit 3.

Spin state at t_2 —At time t_2 , the proton in mode 2 (red) scatters with the proton in mode 1 (gray target) at 151 MeV with a center-of-mass scattering angle of 90° . We postselect coincidence events in which the two outgoing protons are registered in two distinct detector arms (centered at $\pm 45^{\circ}$ in the laboratory frame). At this kinematic point, the scattering matrix is well approximated by

$$M_{12} \approx \lambda |\Psi^+\rangle_{12} \langle\Phi^-|_{12}, \quad (\text{S14})$$

where $\lambda = -3.845 - i0.058$ is the dominant matrix element. This operator selects the $|\Phi^-\rangle_{12}$ component from the input state and converts it to $|\Psi^+\rangle_{12}$.

Applying $(M_{12} \otimes \mathbf{1}_3)$ to the state in Eq. (S13), we obtain

$$(M_{12} \otimes \mathbf{1}_3) |\Psi(t_1)\rangle \approx \frac{\lambda}{2} |\Psi^+\rangle_{12} \langle\Phi^-|_{12} \left[|\Phi^-\rangle_{12} \otimes (\alpha|1\rangle_3 + \beta|0\rangle_3) + \dots \right] \\ = \frac{\lambda}{2} |\Psi^+\rangle_{12} \otimes (\alpha|1\rangle_3 + \beta|0\rangle_3). \quad (\text{S15})$$

After normalization, the post-scattering state becomes

$$|\Psi(t_2)\rangle = |\Psi^+\rangle_{12} \otimes (\alpha|1\rangle_3 + \beta|0\rangle_3). \quad (\text{S16})$$

Spin state at t_3 —At time t_3 , after the scattering event, the remote proton 3 (blue) carries the spin state

$$|\tilde{\psi}\rangle_3 = \alpha|1\rangle_3 + \beta|0\rangle_3. \quad (\text{S17})$$

This state is related to the original unknown state $|\psi\rangle_1 = \alpha|0\rangle_1 + \beta|1\rangle_1$ by an interchange of $|0\rangle \leftrightarrow |1\rangle$, which corresponds to an inversion of the quantization axis. For the purpose of verifying teleportation, one can simply account for this axis inversion when comparing the measured polarization of proton 3 with the known polarization of the original target.

Comparison with standard teleportation—In the standard quantum teleportation protocol, Alice performs a complete Bell measurement that can distinguish all four Bell states, and Bob applies one of four possible Pauli corrections ($\mathbf{1}$, X , Z , or XZ) depending on the outcome. In contrast, the nuclear teleportation protocol at 151 MeV implements a *partial* Bell measurement: the scattering amplitude $M \propto |\Psi^+\rangle\langle\Phi^-|$ acts as a filter that selects only events where the two incoming protons in modes 1 and 2 have a $|\Phi^-$ component. This probabilistic selection eliminates the need for Bob to apply different corrections. The trade-off is that the protocol succeeds only for a fraction of events (those where the scattering occurs at the correct kinematics), but successful events are identified by the detection of the scattered protons.

Count-rate estimate. We estimate the spin-teleportation event rate under baseline experimental conditions. The entangled pair (protons 2 and 3) is assumed to be produced via the charge-exchange reaction $p(d, {}^2\text{He})n$ and delivered to a polarized proton target (proton 1). A successful event is tagged by coincident detection of the two scattered protons (1 and 2) at $\pm 45^\circ$ in the laboratory frame within an angular window $\Delta\theta = \pm 1^\circ$, corresponding to $\Delta\Omega = 2\pi[\cos(44^\circ) - \cos(46^\circ)] \simeq 0.155$ sr.

At 151 MeV and 45°_{lab} we take $(d\sigma/d\Omega)_{\text{lab}} \simeq 10.6$ mb/sr [53], giving $\sigma_{\text{acc}} \simeq (d\sigma/d\Omega)_{\text{lab}}\Delta\Omega \simeq 1.64$ mb. For a 1 cm thick liquid-hydrogen target with areal density $N_t \simeq 4.24 \times 10^{22}$ cm $^{-2}$, the scattering (tagging) probability is $P_{\text{scatter}} \simeq \sigma_{\text{acc}}N_t \simeq 7.0 \times 10^{-5}$ per incident proton-2 on target-1. Assuming an incident entangled-proton flux of $\dot{N}_{\text{pair}} \simeq 6 \times 10^7$ s $^{-1}$, the resulting spin-teleportation event rate is $\dot{N}_{\text{tel}} \simeq \dot{N}_{\text{pair}}P_{\text{scatter}} \simeq 4.2 \times 10^3$ s $^{-1}$, which is sufficient to accumulate statistically significant statistics for verification at rates of $\sim 10^3$ – 10^4 s $^{-1}$.

Extension to mixed states—The analysis above assumes that the target proton carries a pure spin state. Here we generalize the protocol to the case where the target proton is in a mixed state, which is more realistic for experimental implementations.

A general mixed state of the target proton can be written as

$$\rho_1 = \sum_i p_i |\psi_i\rangle_1 \langle\psi_i|_1, \quad (\text{S18})$$

where $p_i \geq 0$, $\sum_i p_i = 1$, and each $|\psi_i\rangle_1 = \alpha_i |0\rangle_1 + \beta_i |1\rangle_1$ is a normalized pure state with $|\alpha_i|^2 + |\beta_i|^2 = 1$. The initial three-proton density matrix at time t_1 is

$$\rho(t_1) = \rho_1 \otimes |\Psi^-\rangle_{23} \langle\Psi^-|_{23} = \sum_i p_i |\psi_i\rangle_1 \langle\psi_i|_1 \otimes |\Psi^-\rangle_{23} \langle\Psi^-|_{23}. \quad (\text{S19})$$

At time t_2 , the scattering operator $M_{12} \otimes \mathbf{1}_3$ acts on the system. Since the scattering transformation is linear, we can apply it to each term in the mixture separately. For each pure-state component, following the derivation in the previous subsections, we have

$$(M_{12} \otimes \mathbf{1}_3) (|\psi_i\rangle_1 \langle\psi_i|_1 \otimes |\Psi^-\rangle_{23} \langle\Psi^-|_{23}) (M_{12}^\dagger \otimes \mathbf{1}_3) \propto |\Psi^+\rangle_{12} \langle\Psi^+|_{12} \otimes |\tilde{\psi}_i\rangle_3 \langle\tilde{\psi}_i|_3, \quad (\text{S20})$$

where $|\tilde{\psi}_i\rangle_3 = \alpha_i |1\rangle_3 + \beta_i |0\rangle_3$ is the teleported state corresponding to the input $|\psi_i\rangle_1$.

Summing over all components and normalizing, the post-scattering density matrix becomes

$$\rho(t_2) = |\Psi^+\rangle_{12} \langle\Psi^+|_{12} \otimes \tilde{\rho}_3, \quad (\text{S21})$$

where the reduced density matrix of proton 3 is

$$\tilde{\rho}_3 = \sum_i p_i |\tilde{\psi}_i\rangle_3 \langle\tilde{\psi}_i|_3. \quad (\text{S22})$$

To relate $\tilde{\rho}_3$ to the original mixed state ρ_1 , we note that each teleported pure-state component $|\tilde{\psi}_i\rangle_3 = \alpha_i |1\rangle_3 + \beta_i |0\rangle_3$ differs from the corresponding input state $|\psi_i\rangle_1 = \alpha_i |0\rangle_1 + \beta_i |1\rangle_1$ only by the interchange $|0\rangle \leftrightarrow |1\rangle$, i.e., an inversion of the quantization axis. Since this transformation applies uniformly to all components in the mixture, the teleported mixed state $\tilde{\rho}_3$ is identical to the original mixed state ρ_1 up to the same axis inversion.

Therefore, the teleportation protocol faithfully transfers the mixed state from the target proton to the remote proton, up to the inversion of the quantization axis. This result confirms that the nuclear teleportation protocol preserves not only the coherent superposition of pure states but also the classical probabilistic mixture encoded in the density matrix.

Kinematic windows for the Bell-triplet transition operator—The triplet-based teleportation scheme relies on the fact that, within a finite kinematic window around (E_\odot, θ_\odot) , the dynamics produces an effective Bell-state transition operator,

$$G_\odot \equiv |\Psi^+\rangle \langle\Phi^-|. \quad (\text{S23})$$

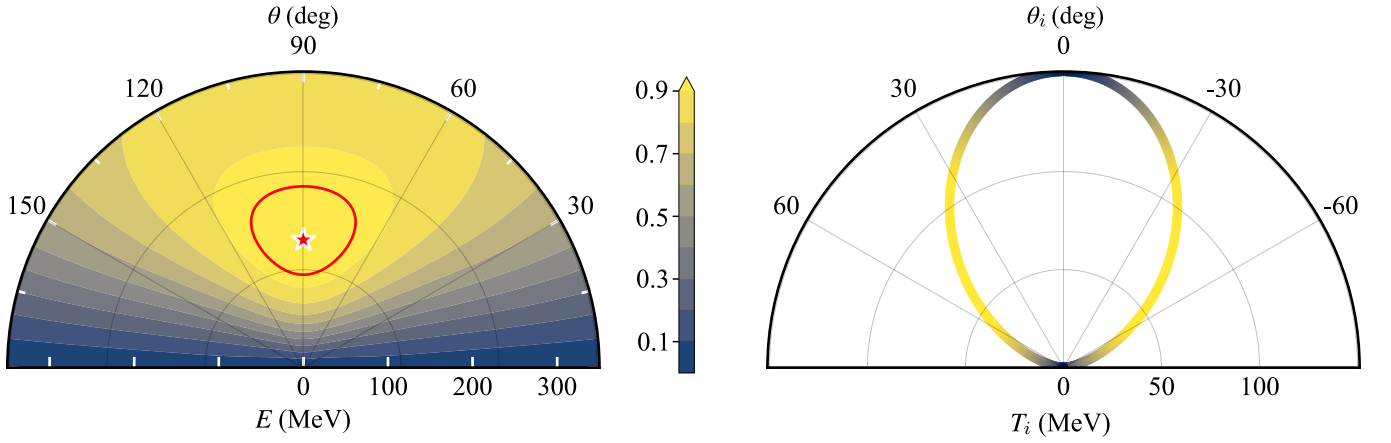


FIG. S4. Kinematic windows for the Bell-triplet transition operator $|\Psi^+\rangle\langle\Phi^-|$. (a) Similarity $\mathcal{S}(E, \theta)$ between the physical pp scattering amplitude $M(E, \theta)$ (from PWA93) and $|\Psi^+\rangle\langle\Phi^-|$ as a function of the beam energy E and center-of-mass angle θ . The red contour encloses the region $\mathcal{S} > 0.95$ (Bell-triplet window), and the star marks (E_\odot, θ_\odot) . (b) Kinematically allowed locus in the (T_i, θ_i) plane (laboratory kinetic energy and scattering angle) for either outgoing proton i at beam energy E_\odot .

To quantify how closely the physical pp scattering amplitude $M(E, \theta)$ approximates the target gate G_\odot , we employ the normalized trace (Hilbert–Schmidt) similarity [63]

$$\mathcal{S}(E, \theta) = \frac{|\text{Tr}[M^\dagger(E, \theta) G_\odot]|}{\sqrt{\text{Tr}[M^\dagger(E, \theta) M(E, \theta)]}}, \quad (\text{S24})$$

which is invariant under an overall rescaling $M \rightarrow \alpha M$ and satisfies $0 \leq \mathcal{S} \leq 1$. Here $M(E, \theta)$ is constructed from the PWA93 phase shifts at beam energy E and center-of-mass scattering angle θ .

Figure S4(a) displays $\mathcal{S}(E, \theta)$ over a broad energy–angle plane. A pronounced high-similarity “island” forms around (E_\odot, θ_\odot) (star), demonstrating that the nuclear interaction naturally generates an amplitude close to G_\odot within a restricted kinematic domain. We define the *Bell-triplet kinematic window* as the region where $\mathcal{S}(E, \theta) > \mathcal{S}_0$, with $\mathcal{S}_0 = 0.95$ (red contour). For clarity, the colormap is saturated at $\mathcal{S} = 0.9$.

For experimental guidance, it is useful to translate this window into laboratory-frame observables. For equal-mass pp scattering in nonrelativistic kinematics, energy–momentum conservation maps a fixed beam energy to a one-dimensional locus in the (T_i, θ_i) plane (laboratory kinetic energy and scattering angle) for each outgoing proton i . Figure S4(b) shows this locus for E_\odot . Its overlap with the Bell-triplet window specifies the coincidence-acceptance band for selecting events that implement the Bell-triplet transition with high fidelity.

V. Proton spin teleportation at $E < 10$ MeV

In this section, we present an alternative teleportation protocol that operates at low energies ($E < 10$ MeV), where S -wave scattering dominates and the scattering amplitude acts as a Bell-singlet projection operator $M \propto |\Psi^-\rangle\langle\Psi^-|$.
Setup—The protocol involves three protons:

- Target proton (gray): The polarized target proton carrying the unknown spin state $|\psi\rangle_1 = \alpha|0\rangle_1 + \beta|1\rangle_1$ to be teleported.
- Incident proton (red): An unpolarized incident proton with kinetic energy below 10 MeV.
- Receiver proton (blue): An unpolarized proton in a liquid hydrogen target, which will receive the teleported state.

Unlike the 151 MeV protocol, this scheme does not require a pre-prepared entangled pair. Instead, the entanglement is generated *in situ* through the first scattering event. A schematic illustration of the protocol is shown in Fig. S5.

Spin state at t_0 —Initially, proton 1 carries the unknown spin state while protons 2 and 3 are completely unpolarized:

$$\rho(t_0) = |\psi\rangle_1 \langle\psi|_1 \otimes \frac{I}{2} \otimes \frac{I}{2}, \quad (\text{S25})$$

where $I/2$ denotes the maximally mixed single-qubit state.

Spin state at t_1 —At time t_1 , the unpolarized incident proton in mode 2 scatters with the unpolarized target proton in the liquid hydrogen target; we postselect events where the two outgoing protons populate two distinct arms, which we then label as modes 2 and 3. At energies below 10 MeV, S -wave scattering dominates, and the scattering amplitude takes the form

$$M_{23} \propto |\Psi^-\rangle_{23} \langle\Psi^-|_{23}. \quad (\text{S26})$$

Applying $(I_1 \otimes M_{23})$ to the initial state and normalizing, the post-scattering state becomes

$$|\Psi(t_1)\rangle = |\psi\rangle_1 \otimes |\Psi^-\rangle_{23}, \quad (\text{S27})$$

where protons 2 and 3 are now maximally entangled in the Bell-singlet state. This entanglement generation through low-energy pp scattering was first exploited in the nuclear Bell test by Laméhi-Rachti and Mittig in 1976.

Expanding this state in the Bell basis for qubits 1 and 2:

$$\begin{aligned} |\Psi(t_1)\rangle = \frac{1}{2} \Big[& |\Phi^+\rangle_{12} \otimes (\alpha|1\rangle_3 - \beta|0\rangle_3) + |\Phi^-\rangle_{12} \otimes (\alpha|1\rangle_3 + \beta|0\rangle_3) \\ & + |\Psi^+\rangle_{12} \otimes (-\alpha|0\rangle_3 + \beta|1\rangle_3) + |\Psi^-\rangle_{12} \otimes (-\alpha|0\rangle_3 - \beta|1\rangle_3) \Big]. \end{aligned} \quad (\text{S28})$$

Spin state at t_2 —At time t_2 , the proton in the selected outgoing arm (mode 2) is directed to scatter with the polarized target proton in mode 1, again at low energy where $M_{12} \propto |\Psi^-\rangle_{12} \langle\Psi^-|_{12}$. This operator projects onto the $|\Psi^-\rangle_{12}$ component of Eq. (S28):

$$(M_{12} \otimes \mathbf{1}_3) |\Psi(t_1)\rangle \propto |\Psi^-\rangle_{12} \otimes (-\alpha|0\rangle_3 - \beta|1\rangle_3). \quad (\text{S29})$$

After normalization, the final state is

$$|\Psi(t_2)\rangle = |\Psi^-\rangle_{12} \otimes (-\alpha|0\rangle_3 - \beta|1\rangle_3). \quad (\text{S30})$$

The remote proton 3 now carries the spin state $-(\alpha|0\rangle_3 + \beta|1\rangle_3)$, which is identical to the original unknown state $|\psi\rangle_1$ up to an irrelevant global phase.

Comparison with the 151 MeV protocol—The low-energy protocol differs from the 151 MeV protocol in several key aspects:

1. *Entanglement source*: The low-energy protocol generates entanglement on-the-fly through the first pp scattering, whereas the 151 MeV protocol requires a pre-prepared entangled pair from, e.g., the $p(d, 2p)n$ reaction.
2. *Scattering operator*: At $E < 10$ MeV, the amplitude $M \propto |\Psi^-\rangle\langle\Psi^-|$ acts as a projection operator onto the Bell-singlet state. At 151 MeV and 90° , the amplitude $M \propto |\Psi^+\rangle\langle\Psi^-|$ acts as a transition operator between different Bell states.
3. *Final state transformation*: In the low-energy case, the teleported state matches the original state exactly (up to a global phase). In the 151 MeV case, the teleported state differs by an interchange $|0\rangle \leftrightarrow |1\rangle$, corresponding to an inversion of the quantization axis.

Both protocols implement probabilistic teleportation: successful events are heralded by the detection of the scattered proton pair at the appropriate kinematics.

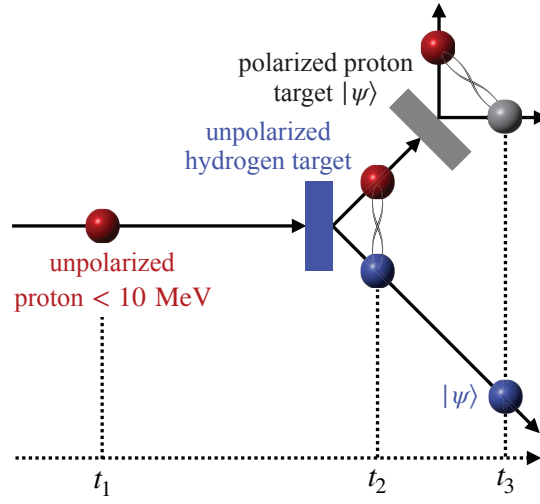


FIG. S5. Schematic of the proton spin teleportation protocol at $E < 10$ MeV. An unpolarized proton (red) with kinetic energy below 10 MeV scatters off an unpolarized liquid hydrogen target (blue rectangle) at time t_1 , generating a spin-entangled proton pair via S -wave dominated scattering. At time t_2 , one of the scattered protons (red) interacts with a polarized proton target (gray) carrying the unknown spin state $|\psi\rangle$. The second low-energy scattering projects the red and gray protons onto the Bell-singlet state, completing the teleportation. At time t_3 , the remote blue proton carries the teleported spin state $|\psi\rangle$.